Journal of Power Sources 423 (2019) 367–379

Contents lists available at ScienceDirect

Journal of Power Sources

journal homepage: www.elsevier.com/locate/jpowsour

New fast charging method of lithium-ion batteries based on a reduced order electrochemical model considering side reaction

Yilin Yin[a], Yang Hu[a], Song-Yul Choe[a,*], Hana Cho[b], Won Tae Joe[b]

[a] Mechanical Engineering, 1418 Wiggins Hall, Auburn University, AL, 36849, USA
[b] Battery R&D, 3 road 36, Janggun maeul, Gwacheon, Kyungkido, 427-710, South Korea

HIGHLIGHTS

- Proposal of a new fast charging method based on a reduced electrochemical model.
- Analysis of effects of C-rates and SOC on degradation for CC/CV charging.
- Design and comparison of charging protocols using different limiting factors.
- Verification of charging method in real time using the Battery-In-The-Loop system.
- Reduction of the charging time more than 40% while maintaining the aging speed.

ARTICLE INFO

Keywords:
Lithium-ion battery
Fast charging method
Reduced order electrochemical model
Side reactions
Charging time
Degradation speed

ABSTRACT

The increase of charging current can reduce the charging time, however, this increased charging current accelerates the speed of degradation and heat generation. There have been many suggested classical charging methods that include constant current and constant voltage, pulse charging or a combination, but few of these charging methods have been designed by considering the fundamental mechanisms of ion transport, chemical reactions, and intercalation process. Therefore, in order to minimize degradation rate and reduce charging time simultaneously, a charging method was designed for the beginning of life of battery by considering different limiting factors such as surface ion concentrations, state of charge, cutoff voltage, and side reaction rate, which generates different charging protocols. The designed protocols were implemented in real time using the Battery-In-The-Loop (BIL) system. Experimental results have shown that the proposed charging methods can reduce about half of the charging time compared with 1C CC/CV normal charging method recommended by manufacturer. Fast charging protocol considering side reaction rate and ion concentration yields the best performance among others in that the charging time can be reduced more than 40% compared with the normal charging with a degradation rate comparable with that of the normal charging up to 100 cycles.

1. Introduction

Lithium-ion batteries are among the most promising energy storage devices used for electric vehicles (EVs) because of their high power and energy density. The battery is charged from different power sources such as an AC grid or electric motors driven by an engine or in regenerative mode. Currently, there are two technical barriers to overcome for rapid and wide acceptance of EVs in markets. These are a relatively short driving range and a long charging time. The driving range can be extended by the installation of more batteries, but this leads adversely to an increase of charging time. There have been several attempts to reduce the charging time with high power chargers such as DC fast charging (50 kW), a supercharger (140 kW), or extreme fast charging (350 kW) [1]. The resulting increased charging current accelerates degradation, which significantly reduces the lifespan of the batteries and generates substantially more heat. Thus, the challenging issues of designing a fast charging method are not only to reduce the charging time but also to keep the degradation and heat generation as low as possible.

1.1. Review of charging methods

Design of charging methods for lithium-ion batteries should

* Corresponding author.
E-mail addresses: yzy0037@tigermail.auburn.edu (Y. Yin), yzh0058@tigermail.auburn.edu (Y. Hu), choeson@auburn.edu (S.-Y. Choe), chohana@lgchem.com (H. Cho), wontaejoe@lgchem.com (W.T. Joe).

https://doi.org/10.1016/j.jpowsour.2019.03.007
Received 11 May 2018; Received in revised form 29 January 2019; Accepted 2 March 2019
Available online 28 March 2019
0378-7753/

Nomenclatures

A	sandwich area of the cell (cm^2)
a_s	specific surface area of electrode (cm^{-1})
BIL	Battery-In-the-Loop
c	ion concentration (mol L^{-1})
$C_{ionloss}$	amount of ion loss caused by the side reactions (A h)
D	diffusion coefficient in electrode ($cm^2\ s^{-1}$)
EC	Ethylene Carbonate
EIS	Electrochemical Impedance Spectroscopy
EKF	Extended Kalman Filter
F	Faraday constant (96,487 C mol^{-1})
FOM	Full Order Model
I	current of the cell (A)
i_o	exchange current density (A cm^{-2})
j	reaction rate (A cm^{-3})
L	thickness of micro cell (cm)
l	coordinate along the thickness of micro cell
OCV	Open Circuit Voltage (V)
Q	capacity of the cell (A h)
R	resistance ($\Omega\ cm^2$) or universal gas constant (8.3143 J $mol^{-1}\ K^{-1}$)
R_s	radius of spherical electrode particle (cm)
ROM	Reduced Order Model
r	coordinate along the radius of electrode particle (cm)
SOC	State Of Charge
SEI	Solid Electrolyte Interphase
T	cell temperature (K)
t	time (s)
U_{eq}	equilibrium potential (V)
V_t	terminal voltage of cell (V)
x	stoichiometric number of the anode
y	stoichiometric number of the cathode

Greek symbols

α	transfer coefficient of reaction
δ	thickness (mm)
ε	volume fraction of a porous medium or strain
φ	electric potential (V)
η	surface overpotential of electrode reaction (V)
κ	ionic conductivity (S cm^{-1})
σ	conductivity (S cm^{-1})
τ	total time (s)

Subscripts and Superscripts

a	anodic
aged	aged cell
ave	average value
c	cathodic
e	electrolyte phase
eff	effective
eq	equilibrium
fresh	fresh cell
ion loss	caused by loss of lithium ion
Li	lithium ion
max	maximum
s	solid phase
side	the side reaction
surf	electrode particle surface
-	negative electrode (anode)
+	positive electrode (cathode)

consider various operation aspects given in the battery specification such as capacity, cutoff voltage, maximum temperature, and maximum charging current.

Generally, there are three basic charging methods: constant current (CC), constant power (CP) and constant voltage (CV). The CC charging method uses a constant current, which enables reduction of the charging time, but might overcharge a battery even using a small current. When charged with CP, the current at the beginning is relatively high, which can reduce the charging time, but also cause overcharging. The CV charging can prevent a battery from overcharging but has a substantially lower charging rate on average. Like CC charging, the charging current at a low SOC becomes high, which induces a high temperature rise and a high degradation rate. Combinations of CC with CV or CP with CV charging prevent the overcharging, temperature rise, and high degradation rate, resulting in a constant current constant voltage (CC/CV) charging method or constant power constant voltage (CP/CV) charging method [2,3]. Both charging methods use CC or CP to charge the battery until a cutoff voltage is reached and then use CV mode to fully charge it. In fact, charging currents in the CP/CV method at low SOC is higher than that in the CC/CV method due to the spike in charging current. Therefore, the CC/CV charging method is widely preferred because it prevents the overcharging and limitation of the high charging current at the beginning, which assures safe operation and a lower degradation rate [4].

There are many suggestions for optimization of the CC/CV charging method with respect to the charging time, degradation, heat generation, safety, use of electric equivalent circuit models (EECM), or electrochemical models. The EECM is used to estimate SOC, impedances, and heat generation. The estimated SOC is used to determine the proper transition time from CC to CV mode, which can reduce the total charging time due to the extension of the CC mode [4]. Additionally, in different SOC ranges, different charging C-rates are used to charge the battery, which reduces the charging time while maintaining the degradation speed [5,6]. The inaccuracy of estimated SOC caused by hysteresis can be corrected by restricting the hysteresis [7]. The temperature rise induced by high charging currents is limited by combining a thermal model with the EECM to limit the high degradation rate [8,9].

These charging methods enable reduction of the charging time but do not consider the degradation effects from fundamental mechanisms. As a matter of fact, the EECM does not describe the internal mechanisms taking place during the charging processes such as ion transport, electrochemical reaction, intercalation/deintercalation, and ion diffusion. As a result, it is impossible to perfectly optimize the high charging currents while minimizing the aging speed. The internal processes of a battery can be accurately described using electrochemical principles [10]. A large format pouch-type cell with multiple layers is simplified to a microcell under assumptions that there are no thermal and ion gradients in lateral direction and that the current collectors on each layer have the same potential. The microcell is a sandwich structure that consists of a current collector, a composite anode and cathode, and a separator. It is assumed that electrodes are composed of spherical particles with the same radius, which are in contact with each other. Ions are transported through the plane and are diffused in these particles. The model considering this structure is called a “full order model with pseudo-two-dimensions” or “FOM-P2D”. The FOM-P2D can estimate SOC and anode potentials, which are used in the design of fast charging methods to reduce the charging currents and prevent lithium plating [11]. However, side reactions that represent the main cause of degradation are not considered. In addition, FOM-P2D is inadequate for fast charging due to the high computational time caused by the complex governing equations. When the partial differential equations and

nonlinear equations of the FOM-P2D are simplified to ordinary differential equations and linearized to linear equations, the FOM-P2D becomes a reduced order model (ROM) that can be better embedded in controllers like battery management systems [12,13]. If both electrodes are assumed to be composed of spherical particles of the same size, and current distribution is assumed to be uniform in both electrodes, all of the particles in both electrodes can be replaced with a single spherical particle, which is called "single particle reduced order model" or "ROM-SP" [14]. In order to maximize battery life while fast charging, ROM-SP was used where the charging current profile was optimized by considering limitations of SOC, terminal voltage, anode potential, and temperature [15]. The optimization was solved using a genetic algorithm as a function of cycle number. Similarly, SOC and anode potential derived from ROM-SP were used to prevent lithium plating at a fast charging rate [16]. However, side reactions were not considered.

Even though calculation of ROM-SP is faster than that of ROM-P2D, the ROM-P2D has several advantages in accuracy and particularly in the calculation of the gradient of ion concentration in solid and current distributions. Some researchers suggest using the ROM-P2D to optimize a charging method by considering SOC, surface ion concentration, and temperature rise. Because of the limited temperature rise, battery life is extended [17]. Other researchers suggest limiting anode potential to prevent the formation of lithium plating [18]. However, these researchers did not consider the side reactions dependent upon operating conditions such as SOC, anode potential, ion concentration.

1.2. Effects of charging methods on degradation

1.2.1. Review of aging mechanisms

Charging time can be reduced simply by increasing the charging current. However, an increased charging current not only generates more heat but also accelerates the aging of the battery.

According to investigations on degradation mechanisms conducted with a large format lithium ion polymer battery with NMC/Carbon or LFP/Carbon chemistries, lithium plating and side reactions at the surface of the anode graphite particles are the two major causes for degradation [19,20].

Lithium plating is one of causes for degradation and predominantly occurs under extreme charging conditions, such as high currents [21], low temperatures [22], and overcharging [23]. Since the charging current rate was less than 5C and the operating temperature was 25 °C, effects of lithium plating are not considered, which might cause some discrepancies in the capacity fade.

Side reactions are a reduction process between electrolyte solvent and lithium ions at the anode particle surface. The products of side reactions can form a very thin film that adheres to the surface of the anode particles, which is called a solid electrolyte interphase (SEI) layer. The side reactions take place continuously throughout the battery life because the anode always operates at the potential that is outside the stability window of the electrolyte component; however, as the SEI layer forms, the side reactions begin to slow down [24]. These deposits accumulate on the surface of anode particles and result in a continuous growth of the SEI layer. The layer at the particles located near the separator grows faster than other particles and forms an extra deposit layer [18]. As a result, the ionic resistance of the layers increases, and the accessible surface area and porosity decrease, with power fade being the result. SEI layers are electronic isolators that can completely isolate some particles from electrons if these particles are fully covered by SEI layers, which leads to a loss of active carbon material, finally resulting in capacity fade. In addition to the active carbon material loss, the consumed ions and electrolyte solvents caused by the side reactions are additional factors for capacity fade.

Side reactions are accelerated by operating conditions such as elevated temperatures and high SOC ranges. A high charging current also promotes the side reactions, which is analyzed later. When the temperature rises, the kinetics of lithium ions and electrolyte solvents are increased, resulting in more ions passing through the SEI layer to the interface [24]. Thus, the concentrations of both ions and solvents on the particles' surface increase, which results in a higher side reaction rate.

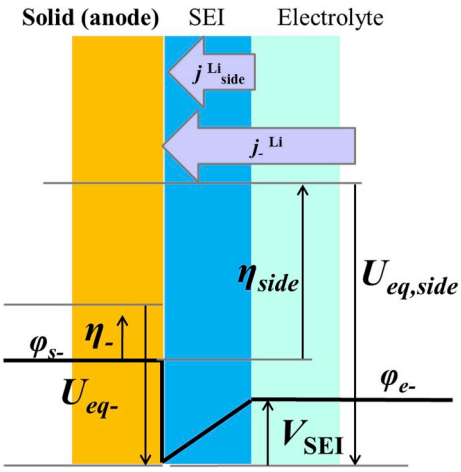

Fig. 1. Schematic diagram of potential relationship at the anode side during charging [31].

The effects of SOC ranges and charging C-rates on the side reactions can be better explained with help of the relationship of potentials at the interface between the anode electrode and the electrolyte. A schematic diagram of the potential relationship at the anode side during charging is depicted in Fig. 1. At charging, two chemical reactions take place, the main and side reactions, with the total reaction rate, j^{Li}_{total}, expressed as a sum of both reaction rates:

$$j^{Li}_{total} = j^{Li}_{-} + j^{Li}_{side} \tag{1}$$

where j^{Li}_{-} and j^{Li}_{side} denote the reaction rates caused by the main and side reactions, respectively.

The reaction rate, j^{Li}_{-}, produced by the reaction at the interface between anode and electrolyte is a function of overpotential, denoted η_{-}, and expressed by the Bulter-Volmer (B-V) equation:

$$j^{Li}_{-} = a_s i_0 \left(\exp\left(\frac{\alpha_a nF}{RT} \eta_{-} \right) - \exp\left(-\frac{\alpha_c nF}{RT} \eta_{-} \right) \right) \tag{2}$$

where a_s is the specific reaction area; α_a and α_c are the anodic and cathodic transfer coefficient, which are both assumed to be 0.5; n is the number of ions participating in the main reaction, which is equal to 1; R is the universal gas constant ($8.3143\,\mathrm{J\,mol^{-1}\,K^{-1}}$); i_0 is the exchange current density; and T is the cell temperature.

The overpotential in the B-V equation above can be expressed as follows:

$$\eta_{-} = \varphi_{s-} - \varphi_{e-} - U_{eq-} - \frac{R_{SEI}}{a_s} j^{Li}_{total} \tag{3}$$

where φ_{s-} and φ_{e-} are the electric potentials of the solid anode particle and electrolyte, respectively.

The equilibrium potential of the anode, U_{eq-}, is a function of the stoichiometric number that is the ratio between ion concentration in its solid phase and its maximum value. R_{SEI} is the resistance of SEI that causes a potential drop across the SEI layer:

$$V_{SEI} = \frac{R_{SEI}}{a_s} j^{Li}_{total} \tag{4}$$

The rate of side reactions, j^{Li}_{side}, is also calculated using the B-V equation:

$$j^{Li}_{side} = -i_{0,side} a_s \exp\left(-\frac{\alpha_{c,side} n_{side} F}{RT} \eta_{side} \right) \tag{5}$$

where n_{side} is the number of ions involved in the side reactions that is

equal to 2. η_{side} is the overpotential of side reactions:

$$\eta_{side} = \varphi_{s\_} - \varphi_{e\_} - U_{eq,side} - \frac{R_{SEI}}{a_s} j_{total}^{Li} \tag{6}$$

where $U_{eq,side}$ is the equilibrium potential of the side reactions, 0.4V [25–28]. The exchange current density of the side reactions, $i_{0,side}$ is a function of two reactants of the side reactions, lithium ions, and EC molecules [29,30]:

$$i_{0,side} = k_{side} \sqrt{c_{s,surf} c_{EC,R_s}} \tag{7}$$

where k_{side} is the kinetic rate constant for the side reactions. $c_{s,surf}$ and c_{EC,R_s} are the concentrations of the lithium ions and the EC molecules at the surface of anode particles, respectively.

$\varphi_{e\_}$ is regarded as the reference to analyze the relationship to other potentials. While the battery is charging, the overpotential, $\eta_{\_}$, is negative because of the negative $j_{\_}^{Li}$ induced by ion transport from the electrolyte to the anode.

When SOC is high, the ion concentration in the anode is high and the equilibrium potential, $U_{eq\_}$, becomes small, and then $\varphi_{s\_}$ also becomes small under the assumption that the overpotential, $\eta_{\_}$, is constant. As shown in Fig. 1, the overpotential for side reaction, η_{side} , decreases, which increases the magnitude of the side reaction rate. Consequently, charging a cell in a high SOC range leads to a high rate of side reactions, which eventually accelerates degradation.

When a high C-rate is used to charge, the magnitude of the overpotential, $\eta_{\_}$, increases according to the B-V equation, which lowers the anode potential, $\varphi_{s\_}$. Since the overpotential for side reactions, η_{side} , is the difference between the anode potential and equilibrium potential, the magnitude of the overpotential for the side reactions increases, which leads to a high side reaction rate.

1.2.2. Review of effects of classical charging methods on charging time and degradation

There are two classical charging methods, CC/CV charging and pulse charging. CC/CV charging is the most commonly used charging method. With a higher C-rate, charging time decreases. However, the charging time cannot be significantly reduced by a high C-rate as that leads to the extension of CV mode [32]. In the CC mode, a higher C-rate leads to a quick increase of SOC, but the terminal voltage reaches the cutoff voltage at a lower SOC. Additionally, a high charging C-rate leads to a high magnitude of the overpotential of the side reactions, which results in an increased side reaction rate and significant reduction of cycle life [33]. More details about the effects of a high charging C-rate on side reactions are analyzed in section 2.2.1. Another option, an increase of cutoff voltage, can also significantly reduce the charging time because the CC charging period is extended and the average charging current in CV mode is increased. However, the increased cutoff voltage accelerates the degradation because the increased charging current leads to higher magnitude of overpotential of the side reactions, which increases the side reaction rate [33]. In conclusion, increasing the charging C-rate or cutoff voltage of the CC/CV charging method does not satisfy the requirements for fast charging: short charging time and slow degradation speed.

While in technical contrast to CC/CV, pulse charging method is also being widely considered for faster charging. The pulse charging method can be categorized into unidirectional and bidirectional pulses depending upon the presence of resting or negative pulses [34]. The charging time is determined by the mean value of the pulse charging current [33,34]. These resting and negative pulses speed up relaxation of ion gradients and the concentration overpotential in the anode composite electrode [35], which suppresses formation of lithium plating. In addition, bidirectional pulse charging with optimized frequency can significantly prevent lithium plating because deposited lithium that dissolves during discharging takes part in the main chemical reactions again [36]. However, other authors claimed no positive or even detrimental effects on the performance and cycle life of lithium-ion batteries [33,37]. For a pulse current with a frequency larger than 10Hz, the lithium-ion battery behaves like a low-pass filter because of the large capacitance of the battery [38], so the degradation is determined by the average value of pulse charging currents. No differences in charging time and degradation speed between pulse charging and CC/CV charging are reported with a pulse frequency of 25Hz [33]. When the frequency is less than 10Hz, the pulse current cannot be completely buffered by the large capacitances of battery, so concentration gradients increase significantly and anode potential becomes more negative, which increases the side reaction rate significantly [38]. Compared with CC/CV charging, pulse currents generate more heat, which causes a higher side reaction rate. When the magnitude of pulse

Table 1
Summary of ROM and FOM.

Cell dynamics	FOM	ROM
Ion concentration in electrode	$\frac{\partial c_s}{\partial t} = \frac{D_s}{r^2}\frac{\partial}{\partial r}\left(r^2\frac{\partial c_s}{\partial r}\right)$ $\frac{1}{r}\frac{\partial c_s}{\partial r}\Big\|_{r=0} = 0$ *and* $D_s\frac{\partial c_s}{\partial r}\Big\|_{r=R_s} = \frac{-j^{Li}}{a_s F}$	$\frac{d}{dt}c_{s,ave} + 3\frac{j^{Li}}{R_s a_s F} = 0$ $\frac{d}{dt}q_{ave} + 30\frac{D_s}{R_s^2}q_{ave} + \frac{45}{2}\frac{j^{Li}}{R_s^2 a_s F} = 0$ $35\frac{D_s}{R_s}(c_{s,surf} - c_{s,ave}) - 8D_s q_{ave} = -\frac{j^{Li}}{a_s F}$
Ion concentration in electrolyte	$\frac{\partial(\varepsilon_e c_e)}{\partial t} = \frac{\partial}{\partial x}\left(D_e^{eff}\frac{\partial}{\partial x}c_e\right) + \frac{1-t_+^0}{F}j^{Li}$ $\frac{\partial c_e}{\partial x}\Big\|_{x=0} = \frac{\partial c_e}{\partial x}\Big\|_{x=L} = 0$	$\dot{\mathbf{c}}_\mathbf{e} = \mathbf{A}^*\cdot\mathbf{c}_\mathbf{e} + \mathbf{B}^*\cdot I$ $\mathbf{y} = \mathbf{C}^*\cdot\mathbf{c}_\mathbf{e} + \mathbf{D}^*\cdot I$
Ohm's law in electrode	$\frac{\partial}{\partial x}\left(\sigma^{eff}\frac{\partial}{\partial x}\varphi_s\right) - j^{Li} = 0$ $-\sigma^{eff}\frac{\partial}{\partial x}\varphi_s\Big\|_{x=0} = -\sigma^{eff}\frac{\partial}{\partial x}\varphi_s\Big\|_{x=L} = \frac{I}{A}$ $\frac{\partial}{\partial x}\varphi_s\Big\|_{x=\delta_-} = \frac{\partial}{\partial x}\varphi_s\Big\|_{x=\delta_-+\delta_{sep}} = 0$	$\frac{\partial}{\partial x}\left(\frac{\partial}{\partial x}\varphi_s\right) = \frac{j^{Li}}{\sigma^{eff}}$ $-\sigma^{eff}\frac{\partial}{\partial x}\varphi_s\Big\|_{x=0} = -\sigma^{eff}\frac{\partial}{\partial x}\varphi_s\Big\|_{x=L} = \frac{I}{A}$ $\frac{\partial}{\partial x}\varphi_s\Big\|_{x=\delta_-} = \frac{\partial}{\partial x}\varphi_s\Big\|_{x=\delta_-+\delta_{sep}} = 0$
Ohm's law in electrolyte	$\frac{\partial}{\partial x}\left(\kappa^{eff}\frac{\partial}{\partial x}\varphi_e\right) + \frac{\partial}{\partial x}\left(\kappa_D^{eff}\frac{\partial}{\partial x}\ln c_e\right) + j^{Li} = 0$ $\frac{\partial}{\partial x}\varphi_e\Big\|_{x=0} = \frac{\partial}{\partial x}\varphi_e\Big\|_{x=L} = 0$	$\frac{\partial}{\partial x}\left(\frac{\partial}{\partial x}\varphi_e\right) + \frac{j^{Li}}{\kappa^{eff}} = 0$ $\frac{\partial}{\partial x}\varphi_e\Big\|_{x=0} = \frac{\partial}{\partial x}\varphi_e\Big\|_{x=L} = 0$
Electrochemical kinetics	$j^{Li} = a_s i_0\left\{\exp\left[\frac{\alpha_a nF}{RT}\eta\right] - \exp\left[-\frac{\alpha_c nF}{RT}\eta\right]\right\}$	$j^{Li} = a_s i_0\frac{n(\alpha_a+\alpha_c)F}{RT}\eta$
SOC	$SOC = \frac{1}{\delta_-}\int_0^{\delta_-}\frac{(c_{s,ave} - c_{s,\max}Stoi_{100})}{c_{s,\max}(Stoi_{100} - Stoi_0)}dx$	

charging decreases, the concentration gradient and ion concentration saturation can be effectively reduced and avoided respectively [34]. Thus, in this paper, only pulse charging with decreased magnitude is employed for the range of high SOC to prevent the ion concentration from exceeding a saturation limit.

2. Design of a fast charging method

Design of a fast charging method takes into account three parts: 1) development of a model that allows for estimation of physical variables such as the ion concentrations and anode potentials in real time and reduction of estimation errors caused by model state error and measurement noises; 2) analysis of the effects of CC/CV charging method on charging time and degradation speed; 3) determination of the magnitude of current rate and duration of pulses considering ion concentration, cutoff voltage, and side reaction rate.

2.1. Reduced order model with EKF

A pouch-type lithium ion polymer cell is made of stacked single microcells that are connected in parallel by current collectors. The micro cell has a sandwich structure in the thickness direction that is composed of composite electrodes and a separator in between. The composite electrodes are made of active materials, electrolytes, and binders. The active materials of the lithium-ion battery are metal oxides for the cathode and carbon for the anode, whose shapes are approximated by a sphere and are distributed uniformly throughout their composite electrodes. When cells are discharged or charged, lithium ions are deintercalated, diffused in the electrode particles, and then are transported through the electrolyte and the separator. Then they are chemically reacted with electrons and active materials at the interface of the electrode particles, then diffused and intercalated into the lattice structure. The electrons flow through an external circuit and complete the redox process.

The intercalation or deintercalation, diffusion, ion transport, chemical reactions, and the resulting change of potentials are described by a set of coupled nonlinear and partial differential equations (PDEs). Four variables of the governing equations can be solved numerically, which is called a full order model (FOM) listed in Table 1. The variables are the ion concentrations and potentials in both the electrodes and the electrolyte. Since the FOM is very computationally intensive, it is inappropriate for use in control purposes, and as such the nonlinearity of equations and the PDE are simplified by linearization and mathematical treatments respectively to a reduced order model (ROM). This ROM, which consists of linear ordinary differential equations (ODEs), can be derived as listed in Table 1. The major mathematical simplifications are carried out for ion concentrations in electrodes and the electrolyte by a polynomial equation and grouped eigenvalues in the state space domain respectively. In addition, if ion concentration in the electrolyte does not significantly affect the reaction current, the equation of phase potential can be also simplified because the second term becomes zero. Furthermore, the nonlinear characteristic of the B-V equation is approximated by a linear equation. The detailed description of the model reduction approaches can be found in Refs. [12,13]. The model parameters used for the ROM are listed in Appendix A.

SOC is defined as a ratio between the total number of ions present in the particles and that of the maximum acceptable ions, where the number of ions at any instant can be calculated based on the average concentration. The dynamic error of the average ion concentration and resulting SOC error given by the initial values are further improved by an extra closed-loop method with an extended Kalman filter (EKF) [39,40] The ROM predicts states and the EKF is used to correct the predicted states and, at the same time, measurement errors.

Since the charging current affects the side reaction rate, it can be limited to suppress the side reaction rate. The ROM-EKF estimates the main chemical reaction rate, j_{-}^{Li}, anode potential, φ_s^- and electrolyte potential, φ_e^- , which are used to estimate the side reaction rate, j_{side}^{Li}, based on Equation (4), Equation (5) and Equation (6).

2.1.1. Validation of ROM-EKF

The battery used in this research is a pouch-type lithium-ion battery with a capacity of 15.7Ah. The active material of the anode and cathode

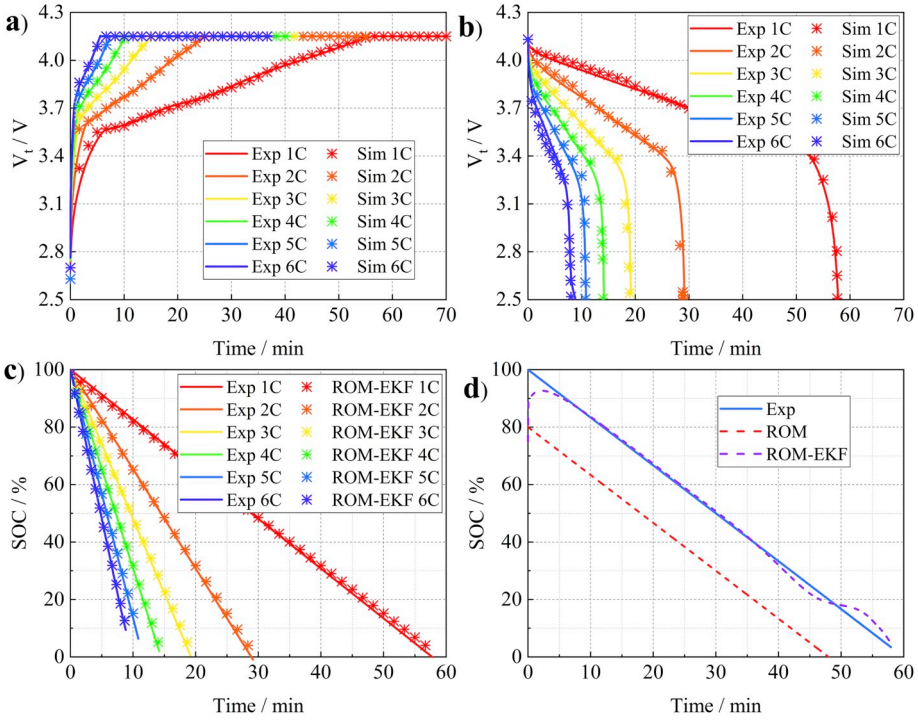

Fig. 2. The simulated and experimental terminal voltages and SOC at different current rates from 0 to 100% SOC and vice versus. a) Terminal voltage at charging; b) Terminal voltage at discharging; c) SOC without initial errors; and d) SOC with initial errors.

is carbon and NMC ($Li[MnNiCo]O_2$), respectively. ROM-EKF is validated against the experimental data at charging and discharging. The current rates are 1C, 2C, 3C, 4C, 5C, and 6C at 25 °C. Even at a high C-rate, the temperature is kept constant by a calorimeter designed in the laboratory that completely rejects the heat generated, so that the effects of the temperature on the charging and discharging characteristics are limited. Details on the calorimeter can be found in Ref. [41].

Simulated and experimental terminal voltages are plotted in Fig. 2a) and b) for comparison, where the starred and solid lines represent simulation and experimental data, respectively. The results show that the terminal voltage of ROM is a fairly good match with those from experiments.

Tracking performance of the EKF for the estimation of SOC is presented in two cases, with and without an initial SOC error, as shown in Fig. 2c) and d). If no initial error is present, the ROM-EKF can estimate the SOC with an absolute error that is less than 5%. Even with a 20% initial SOC error, the ROM-EKF can track the SOC within 100s, but with a little bit of overshoot that can be further optimized by proper selection of the error covariance matrices of the EKF.

2.2. Design of a fast charging method

The CC/CV charging method is the simplest and most widely used charging method. However, increasing the charging current alone cannot significantly reduce the charging time because of the extended duration of the CV charging. In addition, the increased charging current accelerates the degradation of the battery. Thus, before proposing a new charging method, effects of CC/CV charging on the charging time and degradation, specifically side reactions, are first analyzed.

2.2.1. Analysis of effects of CC/CV charging method on charging time and side reactions

2.2.1.1. Charging time. The charging time up to 100% SOC is determined by two factors: the C-rate applied during the constant current range and the cutoff voltage during the constant voltage range. Effects of different C-rates on SOC and charging time in CC mode were studied experimentally using the pouch-type cell, as plotted in Fig. 3a) and b), where the cutoff voltage was set to be 4.15 V. As expected, a high charging C-rate reduces the charging time, but the terminal voltage reaches the cutoff voltage of 4.15V even at a lower SOC because of the high overpotential and the resulting limitation by the cutoff voltage. Thus, the maximum SOC to be charged at a given charging C-rate during CC mode is limited and their relationship is inversely proportional to the C-rate.

The effects of CC with the CV mode on charging time were also studied experimentally, where a cell is charged from 0% to 100% SOC. The C-rate was varied from 0.5 C to 7 C and the cutoff voltage was 4.15V. The charging time as a function of charging C-rates and the ratio between the charging time by CV and CC/CV are plotted in Fig. 3c) and d). If the C-rates are less than 1.5C, the charging time is significantly reduced even with a slight increase in the charging C-rate and is still reduced with C-rates between 1.5C and 4.5C, but no more, even with the higher C-rates. As shown in Fig. 3 d), the ratio of charging time between CV and CC/CV increases as the charging C-rate is increased because the higher the charging current is, the larger the portion of the SOC in CV mode is. Consequently, the charging time in CV mode takes longer, which leads to a longer charging time.

2.2.1.2. Side reactions. Effects of CC/CV charging on side reactions are investigated, where SOC range and C-rates are varied. As discussed in the previous section, ion concentration heavily affects side reactions. The surface ion concentration of the solid particles is estimated by using the validated ROM as plotted in Fig. 4 a), where the x axis represents the coordinate in the direction of through-plane of the anode. Each colored curve represents the surface ion concentration of different anode particles at a specific time. At the beginning of charging, the concentrations are uniformly distributed in the electrode (blue curve). As more ions are transported from the cathode, the ion concentration gradually forms a high gradient, reaches the maximum value after several minutes, and then becomes less and finally hits zero around 2200 seconds. The concentration at the interface between the composite anode and the separator at 301 seconds (end of CC

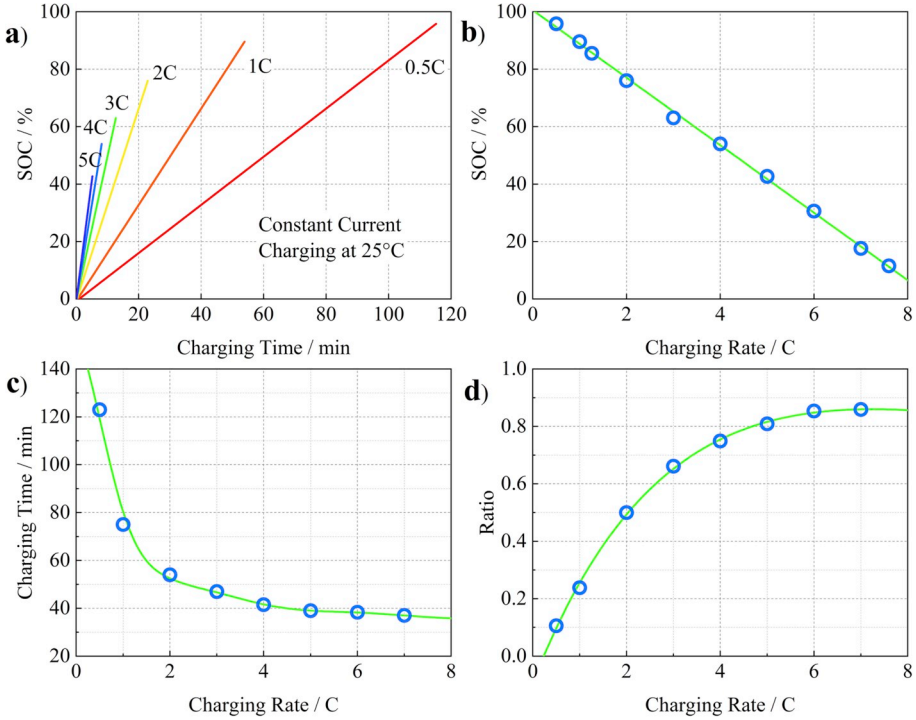

Fig. 3. The charging time and the SOC at different charging C-rates. a) and b) SOC and charging time during CC charging; a) charging time versus time in CC/CV mode; and b) ratio between CV and CC/CV charging time.

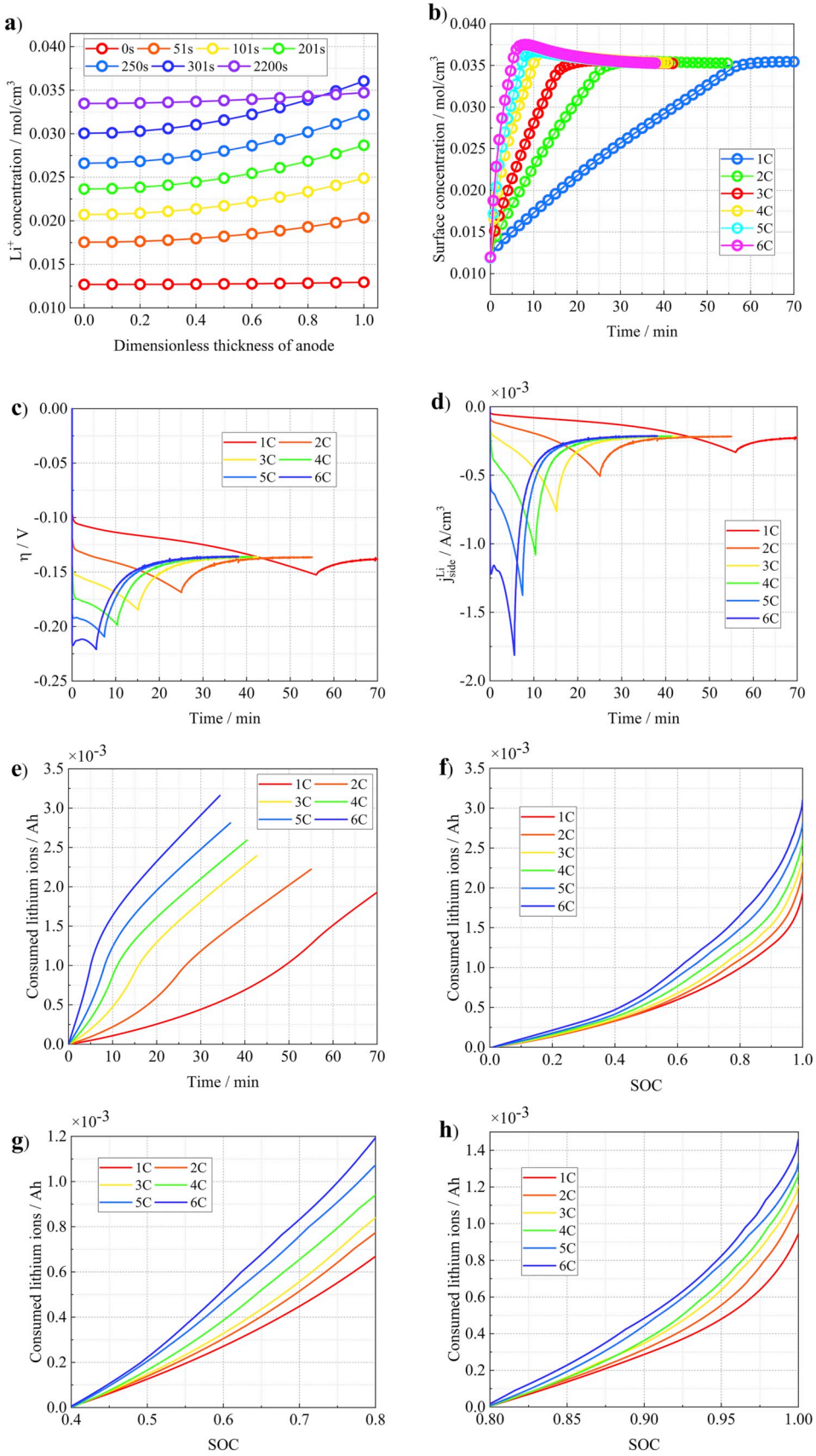

Fig. 4. Simulation results of surface ion concentration of particles and side reactions at different charging C-rates and 25 °C. a) Distribution of surface ion concentration of different particles at different times with 6C rate charging; b) surface ion concentration of the particles next to the separator; c) side reaction overpotential of the particles next to the separator; d) side reaction rate of the particles next to the separator; e) consumed lithium-ion loss vs. time; and consumed lithium-ion loss vs. SOC, f) in whole SOC range, g) in middle SOC range, and h) in high SOC range.

charging) becomes higher than that at 2200s (end of CV charging).

The value of surface ion concentration of a particle is dependent upon the location of the particle due to the limitation of diffusion rate and the gradient of ions in the electrolyte of the composite anode. The closer the particle is to the separator, the higher the surface ion concentration.

The surface concentration of the particle adjacent to the separator in the time domain is plotted in Fig. 4 b). There is an overshoot of the ion concentration during the transit until an equilibrium is reached, when the charging current is larger than 4C. The overshoot is decreased in the CV mode simply because of the decreased charging current. At the steady state when SOC reaches 100%, the concentration converges to a vicinity of a value, which implies that anode particles cannot accept more lithium ions and lithium-ion concentration reaches saturation. The concentration value is 0.035 mol/cm^3 at SOC = 100%, which is chosen as the saturation concentration, c_s^*.

The high ion concentration caused by the overshoot leads to a low equilibrium potential, U_{eq-}, that increases the magnitude of activation overpotential for side reactions and consequently promotes the side reactions. In addition, the excessive ions also increase the exchange current density of side reactions, $i_{0,side}$, according to Eq. (7).

Actually, the side reaction rate is calculated using the B-V equation, as shown in Equation (5). The amount of ion loss, $C_{ionloss}$, that represents the ions consumed by the side reactions is the same as the integration of the side reaction rate, j_{side}^{Li}, over the volume of composite anode and time;

$$C_{ionloss}(\tau) = \int_{x=0}^{\delta_-} \left(\int_{t=0}^{\tau} |j_{side}^{Li}(l,\, t)|dt \right) A dl \tag{8}$$

where $C_{ionloss}$ has a unit of Ah, δ_- is then the thickness of the composite anode, τ is the total operating time, and A is the cross-section area of the cell [18].

Examining these equations, it becomes obvious that the side reaction rate is predominantly affected by the overpotential in the B-V

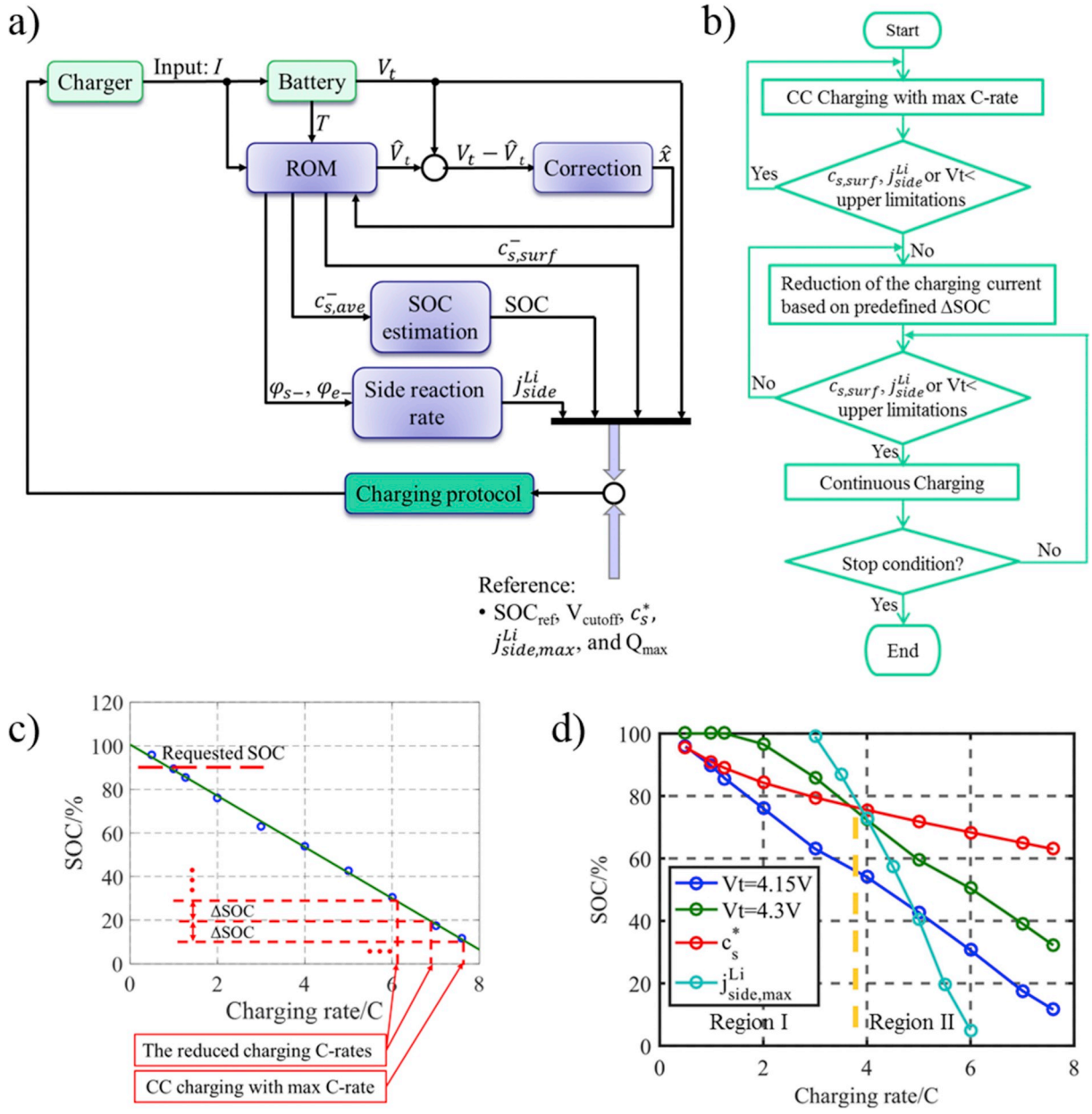

Fig. 5. a) Schematic diagram of a proposed charging method; b) flow chart for the proposing charging method; c) C-rate and SOC limited by the cutoff voltage of 4.15V; d) four limitations to C-rates as a function of SOC.

equation, which is the function of the charging current and the range of SOC, which is calculated and plotted in Fig. 4 c). In addition, the side reaction rate over time and the consumed ion loss versus SOC are plotted in Fig. 4d) and e), and f). The magnitude of the overpotential increases with the increasing charging C-rate until the terminal voltage reaches the cutoff voltage and then decreases in the CV mode. Accordingly, the side reaction rate tends to follow the shape of the overpotential and the consumed ions calculated by Equation (8) increase faster at a higher C-rate. According to the calculation of the ion loss as a function of SOC shows, the ion loss is relatively negligible at a low SOC range, but increases as SOC increases.

When SOC is less than 40%, a high charging current increases the side reaction rate but reduces the charging time, the relationship between charging time and the side reaction rate being almost linear. Therefore, the contribution of the high charging current on degradation is not significant based on Equation (8) and Fig. 4 f). In fact, the increased charging current at the low SOC range does not cause significantly more ion loss in comparison to other ranges but can contribute to a reduction of the charging time. This is only valid assuming a constant cell temperature as the side reaction rate becomes higher at an elevated temperature.

In the middle SOC range, the magnitude between the charging time and overpotential of side reactions becomes nonlinear and the concentration overshoot appears, both of which accelerate the side reactions. Therefore, as the SOC increases, the relationship between charging time and the side reaction rate becomes nonlinear and the magnitude of the slope increases with the increased charging C-rate. As a result, a high charging current largely accelerates the degradation, as shown in Fig. 4 g).

In high SOC range, the side reaction rate is much lower than that of the middle SOC range because of the continuously reduced charging current in CV mode, but the charging time takes longer than in other SOC ranges. In addition, the equilibrium potential becomes lower because of the high ion concentration and then overpotential gets higher, which causes more ion loss, as shown in Fig. 4 h). In this SOC range, the charging C-rate still has a significant effect on lithium-ion loss because of the longer charging time in a high SOC range and a higher side reaction rate caused by higher ion concentration.

2.2.2. Design of the new fast charging method

The design of the new charging method is based on the ROM-EKF that provides variables like average and surface ion concentrations of particles and anode potentials. The variables are used to estimate SOC and side reaction rate. In order to activate the cutoff voltage, the terminal voltage is measured. A block diagram of the proposed fast charging method is depicted in Fig. 5 a). The inputs for the ROM-EKF are the charging current, terminal voltage, and the constant cell temperature. Once the reference values for a requested SOC, cutoff voltage, maximum surface ion concentration, and maximum side reaction rate are given, a charging protocol is generated by comparing the values with those of the estimated and measured and then used to control the charger to generate charging currents.

When a battery is being charged, the requested SOC is one of conditions that stops charging, while other reference values are used to set the upper limitations related to degradation. A flowchart for the designed charging protocol is depicted in Fig. 5 b). At the beginning, a maximum current C-rate is applied until one of the three variables reaches its upper limitation. Upon reaching the limitation, the charging C-rate is reduced and kept as a constant, according to a predefined ΔSOC, which is repeated until the conditions of stop charging are fulfilled.

As an example, experimental data between C-rate and SOC limited by the cutoff voltage of 4.15V is plotted in Fig. 5 c), where the circles represent the experimental data. First, the requested SOC is determined as one of conditions that stops charging. Then the battery is charged with a maximum C-rate of 7.6C, which is the maximum charging current provided by the manufacturer. Once the terminal voltage reaches the cutoff voltage, the charging current is reduced to a lower level, according to the given ΔSOC as shown in Fig. 5 c).

The charging protocol is optimized by considering other limitations that prevent degradation. The first limitation is the cutoff voltage. The manufacturer of the cell recommends 4.3V at the maximum charging C-rate instead of the normal 4.15V. These effects are investigated later. The second one is the calculated maximum surface ion concentration as explained in the previous section. The final one is the maximum side reaction rate selected at 40% SOC based on the result of analysis as shown in Fig. 4 d), where the lithium-ion loss does not significantly increase. In consideration of these limitations, SOC as a function of C-rates is simulated and plotted in Fig. 5 d), which provides an important guideline on how the C-rate at different SOC should be determined for an optimal charging protocol that reduces charging time and at the same time alleviates degradation.

Under the consideration of the limitations, several possible protocols are designed by combining the different limitations listed in Table 2. As the results have shown in Fig. 5 d), charging currents can be limited as SOC increases. At a low SOC range, the maximum side reaction rate is the primary limiting factor of the charging current and then the cutoff voltage of 4.15V is applied up to a middle range of SOC and continuously up to 100% SOC. In CV mode with the cutoff voltage of 4.15V at high SOC ranges, the surface ion concentration can exceed the maximum value and an overshoot occurs. Thus, the limitations are divided into two regions. In region I, the maximum concentration, c_s^*, is the first limitation that should prevent the concentration overshoot. In region II, the other three limitations are used to limit the charging current. Since the overshoot of the surface ion concentration of particles is caused by the mismatch of ions between those transported and those diffused, adding extra resting periods helps reduce the numbers of ions transported and gives the ions extra time to diffuse throughout the particles and to be intercalated [42]. Therefore, the duration of the resting period is determined by considering the gradient of ion concentration in the composite anode. Additionally, high charging currents larger than 5C can make the anode potential negative even at low SOC, which creates favorable conditions for lithium plating. Thus, 5C is selected as the highest C-rate of charging current even though the manufacturer recommends 7.6C.

As an example, simulated results of the charging protocol considering $j_{side,max}^{Li}$ and c_s^* are plotted in Fig. 6 a-d), which includes the current, terminal voltage, surface ion concentration, and the side reaction rate. The surface ion concentration is limited below the maximum allowed saturation concentration, and the side reactions are also limited up until the ion concentration reaches the upper limitation.

Five charging protocols are simulated, and the resulting charging times are summarized in Table 2, where the two classical charging protocols with 1C and 5C CC charging and CV charging by the cutoff voltage of 4.15V are compared. The charging time of 1C CC/CV protocol takes about 71 min to fully charge the battery from 0% to 100% SOC. The designed charging protocols considering a cutoff voltage of 4.3V and 4.15V and the maximum surface ion concentration, FC-4.3V

Table 2
Charging time of different charging protocols.

Charging protocol	CC/CV (1C)	CC/CV(5C)	FC-4.3V	FC-4.15V	FC-SR
Limitation	4.15V	4.15V	4.3V and c_s^*	4.15V and c_s^*	Side reactions and c_s^*
Charging time	71min	38min	31.5min	37.5min	40min

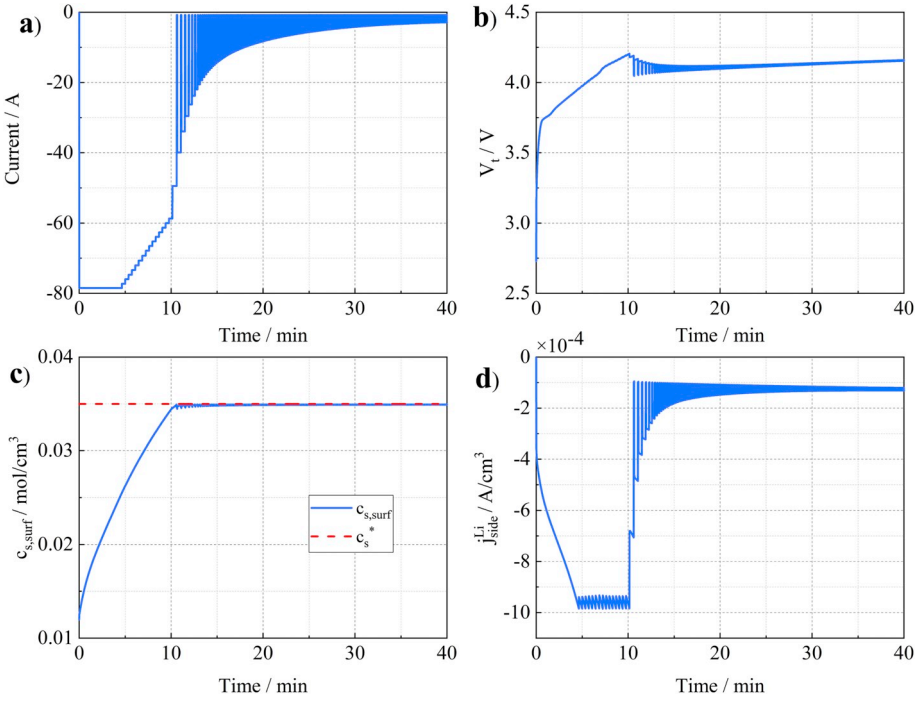

Fig. 6. Simulation results of proposing charging protocol considering maximum side reaction rate and surface ion concentration, a) current; b) voltage; c) surface ion concentration; d) side reaction rate.

and FC-4.15V, reduce the charging time to 44% and 52% of that by the 1C CC/CV charging protocol, respectively, where increased cutoff voltage has contributed to reduce the charging time. The charging time by FC-4.15V is comparable to that of the CC/CV (5C) protocol. The charging time of the protocol that considers side reactions and surface ion concentration takes longer than others because it reduces the total time spent in the CC mode.

Simulation results of the side reaction rate and consumed lithium ions of four charging protocols are plotted in Fig. 7a) and b), where, for brevity, results with 1C are not shown. The area enclosed by the side reaction rate represents the total amount of consumed lithium ions. When the cutoff voltage increases, the CC charging periods become extended, but the magnitude of the side reaction rate becomes higher and the duration is longer. Consequently, the consumed lithium-ion loss increases. If the side reaction rate is further limited, the area becomes smaller and the ion loss becomes significantly reduced, but the charging time is increased.

2.2.3. Experimental assessment of the protocols and analysis

2.2.3.1. Setup of battery-in-the-loop (BIL). The different charging protocols were implemented and experimentally evaluated using BIL that facilitates the operation of a test station with the designed controls in real time. The test station was designed to charge and discharge the battery using a DC power supply and an electronic load that are connected in parallel to the battery and controlled by LabVIEW embedded in a PC. In addition, the battery was placed in a designed calorimeter that dynamically rejects the heat generated by the battery. The calorimeter consists of two thermal electric modules (TEMs), a bipolar power supply, and a control algorithm that determines both magnitude and direction of the current flowing into the TEMs. The TEMs have both cooling and heating functions and regulate the surface temperature of the battery at a set value. The maximum temperature variation becomes less than 1 °C even at a 120A charging current. Thus, this calorimeter allows for a minimization of the effects of the temperature on degradation.

The proposed charging method is implemented in the test station by integrating the ROM-EKF into LabVIEW using a MATLAB script. The

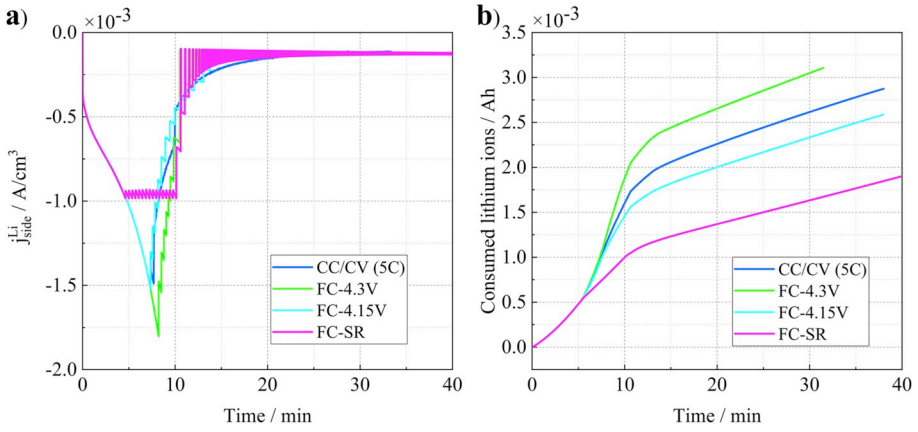

Fig. 7. Side reaction rates and consumed lithium ions of four charging protocols. a) Side reaction rates; b) consumed lithium ions.

ROM-EKF facilitates estimation of the internal variables like SOC, ion concentrations, and the side reaction rate based on the current and terminal voltage, which is used to constrain the charging current and generate the charging protocol for the requested SOC.

The battery used for the experiments is a pouch-type large format lithium-ion cell, whose dimension is about 200 mm × 150 mm × 5 mm. The capacity is 15.7Ah and the operating voltage is in the range of 2.5V–4.15V.

2.2.3.2. Experimental results and analysis. After the implementation of the ROM-EKF in the test station, different charging methods were tested under the same test conditions that were also used for the simulations and then repeated for 100 cycles, where the cell was charged up to 100% SOC and then discharged at a rate of 1C to 0% SOC at 25 °C. The charging time of the five charging protocols in different SOC ranges is summarized in Fig. 8 a). The measured charging times are almost the same as those in the simulations. Compared with the normally recommended 1C CC/CV charging protocol, the other protocols can reduce the charging time by more than half in the low and middle SOC ranges. However, in the high SOC range, the designed charging methods cannot reduce the charging time further. The charging time of the designed charging protocols is almost the same in the low SOC range but differs in the middle SOC range because different limitations are applied. The FC-SR protocol, which limits side reactions, takes the longest of all the designed protocols.

The capacity of the cells is measured after every 10 cycles using the 1C CC/CV charging and discharging method. A dimensionless capacity, Q^*, defined as the ratio of capacity of the aged cell to that of the fresh cell is introduced;

$$Q^* = \frac{Q_{aged}}{Q_{fresh}} \tag{9}$$

The dimensionless capacities of the five charging protocols are plotted in Fig. 8 b). The comparison between FC-4.3V and FC-4.15V shows that an increase in the cutoff voltage accelerates the aging speed substantially. The limitation of the charging current by surface ion concentration helps prevent the capacity fade, which is proved by the comparison between FC-4.15V and CC/CV(5C). The capacity fade of the FC-SR protocol is the least of the designed charging protocols and the closest to that of the CC/CV(1C). Thus, the designed charging methods reduce the charging time and degradation speed. However, the degradation speed of the FC-SR protocol is still slightly higher than that of CC/CV(1C), which is caused by two different factors. Firstly, the lithium-ion loss by the FC-SR protocol is slightly larger than that by CC/CV(1C) in the low SOC range. Secondly, the internal temperature of the battery by the FC-SR protocol is slightly higher than that by CC/CV(1C) because of more heat generated although the surface temperature is kept constant by the calorimeter.

Additionally, the impedances at different charging protocols measured by the EIS are plotted in Fig. 8c) and d). The left intercept between the impedance spectrum and the x-axis at high frequency represents the ohmic resistance and the radius of the first semi-circle represents the SEI resistance. Both of them were extracted using an EIS equivalent circuit model [43]. The growth of both resistances is directly related to power fade. The ohmic resistance of different charging protocols is almost the same as that of the fresh cell, which implies that the side reactions do not contribute to an increase of the ohmic resistance at the BOL. The growth of the SEI resistance after 100 cycles was dependent upon protocols, where the SEI resistance by the FC-SR is comparable to that of CC/CV(1C).

3. Conclusion

An optimization of a fast charging method was proposed that considered charging time and degradation at the beginning of life of battery. Effects of an increase in C-rates, cutoff voltages and internal variables on degradation were identified and analyzed. In order to find an optimal charging protocol, the two internal variables, surface ion

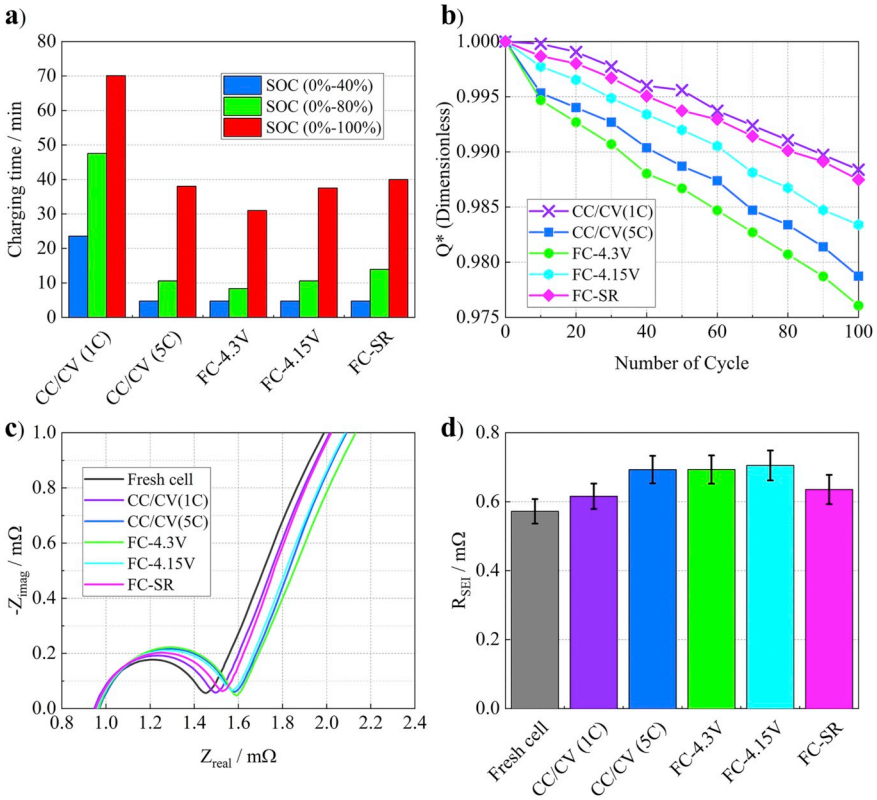

Fig. 8. Comparison of five charging protocols. a) Charging time; b) capacity fade; c) the impedance spectrum measured by EIS; d) the estimated SEI resistance.

concentration and side reaction rate, were estimated by using a reduced order electrochemical model along with an extended Kalman filter. The maximum surface ion concentration and side reaction rate were used to limit the charging currents. The method was implemented in a BIL system and tested for 100 cycles, which verified the protocol with the least capacity and power fade.

Here is a summary of major findings.

- Effects of different amplitudes of charging C-rates on the charging time and side reactions in CC/CV charging are different depending upon SOC ranges. In the low SOC range, high charging C-rates increase the side reaction, but reduce the charging time, so that the contribution of the amplitude of charging C-rates on aging speed is not significant. In middle and high SOC ranges, the charging C-rate has a significantly greater influence on aging speed.
- The proposed charging method was designed using ROM-EKF with a side reaction rate model, where cutoff voltage, saturation of ion concentration, and maximum side reaction rate are used to limit the charging currents. The method reduces about half of the charging time compared with the normal 1C CC/CV charging protocol. Increased cutoff voltage decreases the charging time but increases the capacity and power fade substantially. The limitation of charging current by surface ion concentration helps prevent the capacity and power fade. The charging method limited by surface ion concentration and side reaction rate has shown the best performances with respect to charging time and degradation.

Future work includes effects of charging on lithium plating and heat generation.

Acknowledgement

This project is funded by LG Chem Ltd. The authors do appreciate the financial support and technical discussions.

Appendix A. List of model parameters (a: manufacturers; b: tuning with the model; c: literature).

Category	Parameter	Negative electrode	Separator	Positive electrode	Source
Design specifications (geometry and volume fractions)	Thickness, δ (cm)	$50*10^{-4}$	$25.4*10^{-4}$	$36.4*10^{-4}$	a
	Particle radius, R_s (cm)	$1*10^{-4}$		$1*10^{-4}$	a
	Active material volume fraction, ε_s	0.58		0.5	a
	Polymer phase volume fraction, ε_p	0.048	0.5	0.11	a
	Conductive filler volume fraction, ε_f	0.04		0.06	a
Lithium-ion concentration	Porosity, ε_e	0.332	0.5	0.33	a
	Maximum solid phase concentration, $c_{s,\,max}$ (mol cm^{-3})	$16.1*10^{-3}$		$23.9*10^{-3}$	b
	Stoichiometry at 0% SOC: *Stoi*0	0.126		0.936	b
	Stoichiometry at 100% SOC: *Stoi*100	0.676		0.442	b
	Average electrolyte concentration, c_e (mol cm^{-3})	$1.2*10^{-3}$	$1.2*10^{-3}$	$1.2*10^{-3}$	a
Kinetic and transport properties	Exchange current density coefficient, k_{i0} (A cm^{-2})	12.9		6.28	c [12]
	Charge-transfer coefficient, α_a, α_c	0.5, 0.5		0.5, 0.5	c [13]
	Solid phase conductivity, σ (S cm^{-1})	1		0.1	c [13]
	Electrolyte phase Li^+ diffusion coefficient, D_e (cm^2 s^{-1})	$2.6*10^{-6}$	$2.6*10^{-6}$	$2.6*10^{-6}$	c [13]
	Solid phase Li^+ diffusion coefficient, $D_{s,0}$ (cm^2 s^{-1})	$3*10^{-12}$		$5.55*10^{-12}$	b
	Activation energy of D_s, $E_{a,D}$ (J mol^{-1})	$4.5*10^4$		$4.5*10^4$	b
	Film resistance of SEI layer, $R_{SEI,0}$(Ω cm^2)	1000			b
	Activation energy of R_{SEI}, $E_{a,R}$ (J mol^{-1})	$3.8*10^4$			b
	Bruggeman's porosity exponent, p	1.5	1.5	1.5	c [13]
	Electrolyte phase ionic conductivity, κ (S cm^{-1})	$15.8c_{e^*}\exp(-13472c_e^{1.4})$	c [13]		
	Li^+ transference number, t_+^0	0.363	0.363	0.363	c [13]
Equilibrium potential	Negative electrode (V)	$U_-(x) = 8.00229 + 5.0647x - 12.578x^{\frac{1}{2}} - 8.6322 * 10^{-4}x^{-1} + 2.1765 * 10^{-5}x^{\frac{3}{2}} - 0.46016 * \exp(15 * (0.06 - x)) - 0.55364 * \exp(-2.4326 * (x - 0.92))$ where $x = c_{s,surf}^-/c_{s,max}^-$			c [13]
	Positive electrode (V)	The difference between OCV and the equilibrium potential of the negative electrode			
Side reactions $U_{eq,\,side}$ (V)	Equilibrium potential of side reactions,	0.4			c [25–28]
	Kinetic rate constant for side reactions, k_{side} (A cm mol^{-1})	$3.07*10^{-8}$			b
	Cathodic symmetric factor of side reactions, $\alpha_{c,side}$	0.7			[18]

References

[1] https://energy.gov/eere/articles/pump-charge-extreme-fast-charging, (Jan. 2017).
[2] R.C. Cope, Y. Podrazhansky, The art of battery charging, Battery Conference on Applications and Advances, 1999. The Fourteenth Annual, IEEE, 1999, pp. 233–235.
[3] S.S. Zhang, The effect of the charging protocol on the cycle life of a Li-ion battery, J. Power Sources 161 (2) (2006) 1385–1391.
[4] J.S. Moon, J.H. Lee, I.Y. Ha, T.K. Lee, C.Y. Won, An efficient battery charging algorithm based on state-of-charge estimation for electric vehicle, Electrical Machines and Systems (ICEMS), 2011 International Conference on, IEEE, 2011, pp. 1–6.
[5] T. Wu, Q. Cao, L. Liu, Q. Xiao, X. Wang, Research on the fast charging of VRLA, Indones. J. Electr. Eng. Comput. Sci. 10 (7) (2012) 1660–1666.
[6] T.T. Vo, X. Chen, W. Shen, A. Kapoor, New charging strategy for lithium-ion batteries based on the integration of Taguchi method and state of charge estimation, J. Power Sources 273 (2015) 413–422.
[7] S.J. Huang, B.G. Huang, F.S. Pai, Fast charge strategy based on the characterization and evaluation of LiFePO4 batteries, IEEE Trans. Power Electron. 28 (4) (2013) 1555–1562.
[8] C. Zhang, J. Jiang, Y. Gao, W. Zhang, Q. Liu, X. Hu, Charging optimization in lithium-ion batteries based on temperature rise and charge time, Appl. Energy 194 (2017) 569–577.
[9] B.J. Huang, P.C. Hsu, M.S. Wu, P.Y. Ho, System dynamic model and charging control of lead-acid battery for stand-alone solar PV system, Sol. Energy 84 (5) (2010) 822–830.
[10] M. Doyle, J. Newman, The use of mathematical modeling in the design of lithium/polymer battery systems, Electrochim. Acta 40 (1995) 13–14 2191-2196.
[11] R. Klein, N.A. Chaturvedi, J. Christensen, J. Ahmed, R. Findeisen, A. Kojic, Optimal charging strategies in lithium-ion battery, American Control Conference (ACC), 2011, IEEE, 2011, pp. 382–387.
[12] X. Li, M. Xiao, S.Y. Choe, Reduced order model (ROM) of a pouch type lithium polymer battery based on electrochemical thermal principles for real time applications, Electrochim. Acta 97 (2013) 66–78.
[13] K.A. Smith, C.D. Rahn, C.Y. Wang, Control oriented 1D electrochemical model of lithium ion battery, Energy Convers. Manag. 48 (9) (2007) 2565–2578.
[14] J. Li, N. Lotfi, R.G. Landers, J. Park, A single particle model for lithium-ion batteries with electrolyte and stress-enhanced diffusion physics, J. Electrochem. Soc. 164 (4) (2017) A874–A883.
[15] S.K. Rahimian, S.C. Rayman, R.E. White, Maximizing the life of a lithium-ion cell by optimization of charging rates, J. Electrochem. Soc. 157 (12) (2010) A1302–A1308.
[16] J. Liu, G. Li, H.K. Fathy, A computationally efficient approach for optimizing

lithium-ion battery charging, J. Dyn. Syst. Meas. Control 138 (2) (2016) 021009.
[17] S. Pramanik, A. Sohel, Electrochemical model based charge optimization for lithium-ion batteries, J. Power Sources 313 (2016) 164–177.
[18] Z. Chu, X. Feng, L. Lu, J. Li, X. Han, M. Ouyang, Non-destructive fast charging algorithm of lithium-ion batteries based on the control-oriented electrochemical model, Appl. Energy 204 (2017) 1240–1250.
[19] R. Fu, S.Y. Choe, V. Agubra, J. Fergus, Development of a physics-based degradation model for lithium ion polymer batteries considering side reactions, J. Power Sources 278 (2015) 506–521.
[20] D. Aurbach, D.L. Mikhail, L. Elena, S. Alexander, Failure and stabilization mechanisms of graphite electrodes, J. Phys. Chem. B 101 (12) (1997) 2195–2206.
[21] X. Yang, Y. Leng, G. Zhang, S. Ge, C. Wang, Modeling of lithium plating induced aging of lithium-ion batteries: transition from linear to nonlinear aging, J. Power Sources 360 (2017) 28–40.
[22] H. Ge, T. Aoki, N. Ikeda, S. Suga, T. Isobe, Z. Li, Y. Tabuchi, J. Zhang, Investigating lithium plating in lithium-ion batteries at low temperatures using electrochemical model with NMR assisted parameterization, J. Electrochem. Soc. 164 (6) (2017) A1050–A1060.
[23] W. Lu, C.M. López, N. Liu, J.T. Vaughey, A. Jansen, Overcharge effect on morphology and structure of carbon electrodes for lithium-ion batteries, J. Electrochem. Soc. 159 (5) (2012) A566–A570.
[24] P. Verma, P. Maire, P. Novák, A review of the features and analyses of the solid electrolyte interphase in Li-ion batteries, Electrochim. Acta 55 (22) (2010) 6332–6341.
[25] G. Sikha, B.N. Popov, R.E. White, Effect of porosity on the capacity fade of a lithium-ion battery theory, J. Electrochem. Soc. 151 (7) (2004) A1104–A1114.
[26] P. Ramadass, B. Haran, P.M. Gomadam, R. White, B.N. Popov, Development of first principles capacity fade model for Li-ion cells, J. Electrochem. Soc. 151 (2) (2004) A196–A203.
[27] H.J. Ploehn, P. Ramadass, R.E. White, Solvent diffusion model for aging of lithium-ion battery cells, J. Electrochem. Soc. 151 (3) (2004) A456–A462.
[28] M. Safari, M. Morcrette, A. Teyssot, C. Delacourt, Multimodal physics-based aging model for life prediction of Li-ion batteries, J. Electrochem. Soc. 156 (3) (2009) A145–A153.
[29] Y. Zhao, S. Choe, J. Kee, Modeling of degradation effects and its integration into electrochemical reduced order model for Li (MnNiCo) O2/Graphite polymer battery for real time applications, Electrochim. Acta 270 (2018) 440–452.
[30] M.B. Pinson, M.Z. Bazant, Theory of SEI formation in rechargeable batteries: capacity fade, accelerated aging and lifetime prediction, J. Electrochem. Soc. 160 (2) (2013) A243–A250.
[31] R. Fu, Modeling, Validation and Analysis of Degradation Processes of Lithium Ion Polymer Batteries, PhD diss. (2014).
[32] M.F. Hasan, C.F. Chen, C.E. Shaffer, P.P. Mukherjee, Analysis of the implications of rapid charging on lithium-ion battery performance, J. Electrochem. Soc. 162 (7) (2015) A1382–A1395.
[33] P. Keil, A. Jossen, Charging protocols for lithium-ion batteries and their impact on cycle life—an experimental study with different 18650 high-power cells, J. Energy Storage 6 (2016) 125–141.
[34] B.K. Purushothaman, U. Landau, Rapid charging of lithium-ion batteries using pulsed currents a theoretical analysis, J. Electrochem. Soc. 153 (3) (2006) A533–A542.
[35] P.E. De Jongh, P.H.L. Notten, Effect of current pulses on lithium intercalation batteries, Solid State Ionics 148 (3) (2002) 259–268.
[36] M.Z. Mayers, J.W. Kaminski, T.F. Miller III., Suppression of dendrite formation via pulse charging in rechargeable lithium metal batteries, J. Phys. Chem. C 116 (50) (2012) 26214–26221.
[37] F. Savoye, P. Venet, M. Millet, J. Groot, Impact of periodic current pulses on Li-ion battery performance, IEEE Trans. Ind. Electron. 59 (9) (2012) 3481–3488.
[38] M. Uno, K. Tanaka, Influence of high-frequency charge–discharge cycling induced by cell voltage equalizers on the life performance of lithium-ion cells, IEEE Trans. Veh. Technol. 60 (4) (2011) 1505–1515.
[39] X. Li, S.Y. Choe, State-of-charge (SOC) estimation based on a reduced order electrochemical thermal model and extended Kalman filter, American Control Conference (ACC), 2013, IEEE, 2013, pp. 1100–1105.
[40] K.D. Stetzel, L.L. Aldrich, M.S. Trimboli, G.L. Plett, Electrochemical state and internal variables estimation using a reduced-order physics-based model of a lithium-ion cell and an extended kalman filter, J. Power Sources 278 (2015) 490–505.
[41] Y. Yin, Z. Zheng, S.Y. Choe, Design of a calorimeter for measurement of heat generation rate of lithium ion battery using thermoelectric device, SAE Int. J. Altern. Powertrains 6 (2017) 2017-01-1213.
[42] S.Y. Choe, X. Li, and M. Xiao. Rapid battery charging method and system. U.S. Patent 9,197,089, issued November 24, 2015.
[43] R. Fu, S.Y. Choe, V. Agubra, J. Fergus, Development of a physics-based degradation model for lithium ion polymer batteries considering side reactions, J. Power Sources 278 (2015) 506–521.